scientific reports

Check for updates

OPEN

The effect of copper on the antifungal activity of polyethyleneimines against quiescent conidia and germlings of *Aspergillus nidulans*

Dimitris Tsiourvas[1]✉, Zili Sideratou[1], Eleni Mavrogonatou[2], Dimitris Kletsas[2], Vicky Sophianopoulou[3]✉ & Spiros Gerostathis[3]

The increase in the number of immunocompromised individuals combined with the severity of fungal infections in the general population has contributed to a significant increase in opportunistic fungal infections, which are often associated with high mortality rates. Although effective, existing antifungal drugs operate via a narrow range of mechanisms, leading to the rapid development of resistance and they primarily target growing host cells. Therefore, the need to develop next-generation antifungal agents that function via a broad range of mechanisms and/or target dormant/quiescent cells is highly important. In the present study, we investigated the characteristics and potential antifungal properties of a series of copper-chelated hyperbranched polyethyleneimines (PEI-Cu) with various molar ratios of Cu^{2+}:primary amino groups of PEI (Cu: N), using the opportunistic pathogen *Aspergillus nidulans* as a model microorganism. Our results showed that PEI-Cu¼ and PEI–Cu$^{1}/_{16}$ complexes with Cu: N molar ratios of 1:4 and 1:16, respectively, retain the fungicidal activity of PEI. Cu^{2+} chelation seemed to delay the internalization of PEI-Cu, but they were found to exhibit apparent fungicidal activity on *A. nidulans* quiescent conidiospores while they affected hyphal growth rate, redox status and mitochondrial network morphology in *A. nidulans* germlings. In addition, no cytotoxic effects were observed on normal human skin fibroblasts at concentrations or incubation times that were entirely inhibitory for *A. nidulans*. Overall, our results suggest that the investigated PEI-Cu complexes are promising antifungals, and their underlying mechanism of action deserves further investigation, especially for use against drug-resistant quiescent fungal cells.

In recent years, the increase and severity of fungal infections overall, especially in immunocompromised patients, have become clearly evident. The surge of pathogenic fungal diseases is attributed, among other things, to the recent pandemic, increasing resistance to antifungal agents, the increased number of severely ill patients or even to climate change and increased international travel[1,2]. Recent studies estimate an annual incidence of 6.5 million invasive fungal infections and 3.8 million invasive fungal deaths, approximately 2.5 million (68%) of which are directly attributable to fungal diseases[3]. Opportunistic fungal pathogens, such as *Candida* and *Aspergillus* species (mainly *Aspergillus fumigatus*), pose severe threats to human health when they infect mostly immunocompromised patients[4]. In addition, a World Health Organization (WHO) 2024 data call was released to collect data on antifungal agents used in preclinical development, highlighting, among other issues, the need for novel antifungal agents[5,6]. Although effective, existing antifungal drugs operate via a narrow range of mechanisms, leading to the rapid development of resistance. Moreover, "persisters", a subpopulation of dormant slow-growing fungal cells, are very tolerant to the systematic antifungal agents currently in use since most of them target growing cells[7]. One type of persistent fungal conidium is found in a particular state of the cell cycle, called quiescence. The development of novel potent antifungals with enhanced safety profiles for humans is

[1]Institute of Nanoscience and Nanotechnology, National Centre for Scientific Research "Demokritos", Agia Paraskevi 15341, Greece. [2]Laboratory of Cell Proliferation and Ageing, Institute of Biosciences and Applications (IBA), National Centre for Scientific Research "Demokritos", Agia Paraskevi 15341, Greece. [3]Microbial Molecular Genetics Laboratory, Institute of Biosciences and Applications (IBA), National Centre for Scientific Research "Demokritos", Agia Paraskevi 15341, Greece. ✉email: d.tsiourvas@inn.demokritos.gr; vicky@bio.demokritos.gr

needed but is also challenging, as human and fungal cells share a number of common biological pathways[8,9]. Current research on novel antifungals has focused primarily on developing agents operating via a broad range of mechanisms. This includes the exploration of small molecules and polymeric compounds of either synthetic or natural origin with reported promising antimicrobial/antibacterial properties[10–13], which also target quiescent fungal cells[13].The mode of action of the latter, which is different from that of currently available small-molecule antifungals, can be attributed to fungal membrane depolarization or membrane permeabilization/rupture, followed by cell entry and subcellular localization, which presumably further interferes with various subcellular functions/biochemical pathways[10,12].

A. nidulans is a well-established model microorganism for genetic and molecular/cell biology studies, but it is extensively used as a tractable and versatile organism for the study of pathogenic fungi. Although this fungus is an opportunistic pathogen that is usually harmless to humans, evidence shows that it is a major cause of invasive aspergillosis (IA) in patients with chronic granulomatous disease (CGD)[14]. In addition, primary cutaneous *A. nidulans* infection has long been reported to occur at sites of skin injury (e.g., at intravenous access catheter sites or at sites associated with burns or surgery), especially in immunocompromised patients[15,16]. Eisosomes, which are lateral compartments of the plasma membrane[17–19] and are involved in fungal persistence and pathogenicity[20], are induced in *A. nidulans* quiescent conidia and germlings upon exposure to high copper concentrations (Sophianopoulou and Athanasopoulos, unpublished data). This induction suggests a role for eisosomes and copper in cellular responses to metal stress and in resilience to antifungals. As a trace element, Cu^{2+} serves as an essential cofactor of enzymes that function in many biological processes, including iron acquisition, antioxidative defense and energy metabolism[21]. However, elevated intracellular Cu^{2+} concentrations are toxic, as Cu^{2+} is well known to promote lipid peroxidation[22]. Additionally, Cu^{2+} has been established as an antimicrobial agent[23] that exerts its effects through multiple mechanisms, including the induction of reactive oxygen species (ROS) production[24]. Therefore, its accumulation should be tightly monitored and maintained at homeostatic levels.

In this context, it should be noted that when the Cu^{2+} concentration becomes limiting, *Saccharomyces cerevisiae* promotes Cu^{2+} import through the activation of the transcription factor Mac1, which induces the transcription of the high-affinity Cu^{2+} membrane transporters Ctr1 and Ctr3[25]. In *S. cerevisiae*, as we have recently shown, the eisosome host Flavodoxin-like proteins (FLPs), enzymes essential for the extramitochondrial regeneration of the antioxidant ubiquinol, counteract lipid peroxidation in parallel with the well-studied system of glutathione (GPX) and thus protect yeast quiescent/persistent cells from ferroptosis[26]. Thus, the role of copper in fungal homeostasis should be considered in the context of the development of new antifungal agents, possibly exploiting copper modulation —for instance, through the use of copper (nano)carriers— as an antifungal strategy.

Among the systematically studied groups of polymers used as antifungal/antimicrobial agents, dendritic polymers, which include dendrimers, dendrons, and hyperbranched polymers, have been extensively investigated for more than fifty years. They are currently recognized as important macromolecular compounds, primarily due to their chemical architecture, which favors the encapsulation of drugs, and their large number of end groups, which, after appropriate functionalization or multifunctionalization, allows tailor-made modification of their structure and properties that can have chemical, biochemical and biological significance[27]. An emerging subclass of macromolecules comprises so-called metallopolymers and, of particular interest, metallodendrimers, metallodendrons and metallohyperbranched polymers. These compounds are macromolecules that contain metals at different sites in the dendritic architecture.

N-donor ligands are among the most frequently employed routes for chelation of metal ions, while among hyperbranched polymers, hyperbranched polyethyleneimine (PEI), either as is or appropriately functionalized, is the primary choice[20]. PEI itself has antimicrobial effects on bacteria[28–30], yeast[30], other fungi[13,31], and other microorganisms, such as algae[32]. Its chemical structure (Fig. 1) favors the formation of strong coordination bonds with labile metal ions, particularly with Cu^{2+} ions, forming blue-colored water-soluble complexes with a stability constant of ca. 10^{16}[18,33,34]. Previous studies of systems based on PEI-Cu complexes revealed that they are characterized by high water solubility and low cell toxicity and can stabilize large quantities of Cu^{2+} through coordination. Additionally, it has been reported that these compounds can cross the plasma membrane of the yeast *Pichia pastoris*[35]. In this context, a functionalized poly(propylene amine) dendrimer —a compound with a

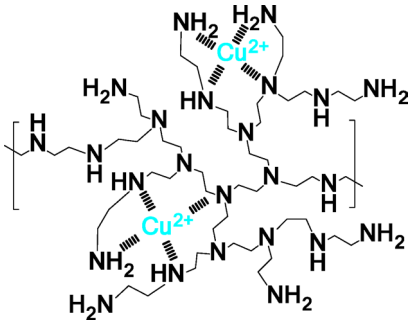

Fig. 1. Schematic illustration of the possible structures of a polyamine–copper compound with a Cu^{2+}:primary amino group molar ratio of 1:4, where $Cu^{2+}$is coordinated with primary, secondary, or tertiary nitrogens.

chemical structure similar to that of PEI— with Cu^{2+} showed good antimicrobial properties, particularly against gram-positive bacteria and the yeast *Candida lipolytica*[36], most likely due to its involvement in cell membrane disruption and permeation.

Our recent findings demonstrated the antifungal activity of PEI and its functionalized derivatives against quiescent/persistent conidia and germlings of *A. nidulans*[13]. Given that copper metabolism is linked to the virulence of fungal cells, since its presence has been shown to increase tolerance to certain antifungals[37], in the present study, we focused on the antifungal properties of PEI-Cu complexes against quiescent fungal conidia and germlings in an effort to diminish their pathogenicity by targeting antioxidant mechanisms important for their survival. We developed a series of PEI-Cu complexes with various Cu: N molar ratios (from 1:32 to 1:4). After the preliminary screening of all PEI-Cu complexes regarding their MIC, we selected PEI-Cu¼ and PEI–Cu$^1/_{16}$ for the rest of our experiments on the comparison of their antifungal activity to that of PEI by monitoring *A. nidulans* growth rate and quiescent conidia survival. PEI-Cu¼ was selected since it has the highest possible molar content of chelated copper, while PEI–Cu$^1/_{16}$, was selected since it has a moderate one, as well as the same MIC to both PEI-Cu 1:8 and 1:32 complexes. The effect of the complexes on the viability of normal human skin fibroblasts was also assessed to determine the possibility of undesirable cytotoxicity. Finally, the mechanism of PEI-Cu complexes' antifungal activity was investigated.

Materials and methods

Chemicals and reagents

Hyperbranched polyethyleneimine (PEI) with an average molecular weight of 25 kDa (Lupasol® WF, 99%, CAS 9002-98-6) was kindly donated by BASF (Ludwigshafen, Germany). Fluorescein isothiocyanate (FITC, CAS 3326-32-7) was purchased from Molecular Probes (Eugene, Oregon, USA). $CuCl_2.2H_2O$ (> 99.0%, Aldrich, Poole, UK) was used as received.

Dulbecco's modified Eagle's medium (DMEM) was purchased from Biosera (Nuaille, France), phenol red-free DMEM and penicillin/streptomycin solution were obtained from Pan Biotech (Aidenbach, Germany), and fetal bovine serum (FBS) and trypsin solution were obtained from Gibco (Thermo Fisher Scientific, Waltham, MA, USA). 3-(4,5-Dimethylthiazol-2-yl)-2,5-diphenyltetrazolium bromide (MTT) and isopropanol were purchased from Sigma–Aldrich Ltd. (Poole, UK). High-purity solvents were obtained from Merck KGaA (Calbiochem®, Darmstadt, Germany).

Synthesis and characterization of fluorescein isothiocyanate (FITC)-labeled hyperbranched polyethyleneimine (PEI-FITC)

The chemical structure of PEI consists of ethylenediamine-type branches bearing primary, secondary and tertiary amine groups (Fig. 1). Inverse-gated decoupling ^{13}C NMR was employed to determine the primary: secondary: tertiary amine ratio of PEI, its branching degree and its degree of polymerization, as described in the literature[38,39]. The ratio of primary to secondary to tertiary amines of PEI was 1.00:1.18:1.01, the branching degree was 0.68, and the average number of primary amino groups per macromolecule was 183[13].

Fluorescein isothiocyanate-labeled PEI (PEI-FITC) was prepared following the interaction of PEI with fluorescein isothiocyanate (FITC) at a 10% molar excess in freshly distilled dried dimethylformamide (DMF) in the presence of catalytic amounts of triethylamine for 24 h at room temperature in the dark, after which the mixture was purified as previously described[13]. The hyperbranched derivative/FITC molar ratio was also determined as previously described and found to be 1:1.1.

PEI-Cu and PEI-FITC-Cu complex formation and characterization

To a PEI solution (2 mg mL^{-1}) in phosphate buffer (PB) (pH 7.4, 100 mM), calculated quantities of a $CuCl_2$ solution (20 mg mL^{-1} in water) were slowly added under intense stirring, yielding a series of PEI-Cu complexes with various molar ratios of Cu: primary amino groups of PEI (Cu: N) and, specifically, with 1:3, 1:3.5, 1:4, 1:8, 1:16, and 1:32 molar ratios. Although complex formation manifested from the appearance of an intense blue color occurred simultaneously, the resulting solutions were allowed to react for 24 h at room temperature to ensure that complete equilibrium was reached. In a similar manner, PEI-FITC was employed for the preparation of two PEI-FITC-Cu compounds, notably, PEI-FITC-Cu¼ and PEI-FITC-Cu$^1/_{16}$, which had Cu: N molar ratios of 1:4 and 1:16, respectively.

Cu^{2+} coordination complex formation was subsequently verified via UV–Vis spectroscopy, employing a Cary 100 Conc UV–Visible spectrophotometer (Varian, Inc., Mulgrave, Victoria, Australia). The corresponding spectra were obtained in the wavelength range of 300–900 nm, and the absorption spectral intensity at 632 nm was registered. The apparent hydrodynamic diameter and surface charge of the parent PEI and the PEI-Cu polymers were determined at 25 °C by dynamic light scattering (DLS) and -zetta potential measurements, respectively, by employing a Zetasizer Nano ZS apparatus (Malvern Instruments Ltd., Worcestershire, UK). For these experiments, aqueous solutions of PEI or PEI-Cu (25 mg mL^{-1}, pH = 7.4) were used. For each solution, ten measurements were acquired, and the results were averaged.

A. nidulans strains, media and growth conditions

Minimal media (MM), complete media (CM) and growth conditions for *A. nidulans* were described by Cove DJ, 1966. When necessary, supplements were added at adequate concentrations (https://www.fgsc.net/). For growth experiments, conidiospores were inoculated on solid MM or CM supplemented with the appropriate nitrogen source and incubated at 37 °C for 3–4 days. The morphological mutations of the *A. nidulans* strains were obtained from A.J. Clutterbuck (https://fungidb.org/fungidb/app). The auxotrophic strain *pabaA1* (p-aminobenzoic acid requiring), originating from the wild-type Glasgow FGSC4 strain (https://fungidb.org/fungidb/app/record/dataset/NCBITAXON_227321), was used as a wild-type strain in this study. In brief, the *pabaA1* strain was

grown in MM or CM (pH 6.8) supplemented with 5 mM urea (CAS 57-13-6) as sole nitrogen source, 1% (w/v) glucose (CAS 50-99-7) as sole carbon source and 5 mM p-aminobenzoic acid (PABA, CAS Number: 150-13-0). Conidia in CM were harvested and transferred to 10 mL of a 0.05% Tween-20 (CAS 9005-64-5) sterilized aqueous solution. Conidia suspension was filtered through a Miracloth filter (475855-1R EMD Millipore), and after successive decimal dilutions (1:10), the concentration was calculated using a Neubauer hemocytometer.

Determination of the minimum inhibitory concentration (MIC) of PEI-Cu complexes

The MIC of each PEI-Cu complex was determined in 96-well flat bottom plates (Greiner AG, Austria) using a slightly modified version of the EUCAST E.DEF 9.3 method for molds. Briefly, the assay mixture was prepared by adding 1 volume (0.1 mL) of conidial suspension ($\sim 2 \times 10^5$ conidia mL^{-1} in 0.05% Tween-20) to 1 volume of assay medium [MM DS (Double Strength)] containing the test compound at twofold greater concentrations. Serial dilutions of each compound were prepared in the assay mixture, with final concentrations ranging from 1 to 20 μg mL^{-1}. The plates were sealed with a plastic membrane to reduce evaporation and incubated at 37 °C for 48 h. After incubation, the plates were visually analyzed by assessing the degree of hyphal growth. The concentration of each compound yielding no visible hyphal growth was recorded as the MIC value. Six technical replicates were included in the plate for each concentration, and the experiment was repeated at least five independent times.

Colony formation assay

To investigate the toxicity of the PEI-Cu complexes, a colony forming unit (CFU) assay was used according to a slightly modified protocol described previously[13]. In brief, the assay mixture was prepared as described in Sect. "Determination of the minimum inhibitory concentration (MIC) of PEI-Cu complexes", with a final inoculum concentration of 1×10^5 conidia mL^{-1} and 5 or 50 μg mL^{-1} of each compound (i.e., ~MIC and 10× MIC). The plates were incubated at 37 °C for 2, 4 and 6 h. After incubation, each well (0.2 mL) was diluted 1:10 in Tween-20 (0.01% v/v). One hundred microliters (100 μL) of each suspension were spread onto CM plates, yielding approximately 300 cells per plate, and the plates were incubated for 2–3 days at 37 °C. The number of colonies was then counted for each sample and compared to that of the control sample (no added compounds). Relative cell viability was calculated as the percentage (%) of cell survival relative to the number of colonies formed in the control sample. Six replicates were performed for each compound concentration, and the experiment was independently repeated at least 3 times.

DCF assay for ROS detection

To detect the accumulation of reactive oxygen species (ROS), the 2',7'-dichlorodihydrofluorescein diacetate (H_2DCFDA) assay was used. H_2DCFDA is a widely used fluorescent probe for ROS detection that is cell permeable and nonfluorescent until it is hydrolyzed by intracellular esterases and subsequently oxidized by ROS to form the highly fluorescent dichlorodihydrofluorescein (DCF). In particular, 35 mm Petri dishes containing 2 mL of MM and the appropriate auxotrophy (p-aminobenzoic acid) were inoculated with $\sim 5 \times 10^5$ *pabaA1* conidia mL^{-1} for 14 h at 25 °C. H_2DCFDA (10 μM) was added to each dish, and the dishes were incubated in the dark for at least 45 min at 25 °C. The medium was then replaced with 2 mL of MM containing 5 μg mL^{-1} of each test compound, separately, in the absence or presence of 10 mM of the ROS scavenger N-acetyl cysteine (NAC), and the plates were incubated in the dark for 5–25 min. The treated conidia were observed by epifluorescence microscopy, and ROS accumulation was quantified by calculating the percentage (%) of cells exhibiting DCF fluorescence compared to the total number of cells. Approximately 150 cells were observed in each sample, and the experiment was repeated 3 times ($n = 450$).

Confocal laser microscopy (CLM)

1×10^6 *pabaA1* conidia mL^{-1} in 0.05% (v/v) Tween-20 were cultured in MM supplemented with 5 mM urea and 1% (w/v) glucose as the sole nitrogen and carbon sources, respectively, in 8-well μ-Slides (Ibidi GmbH, Germany). Cells were imaged using a Leica TCS SP5 (Leica Microsystems Ltd., Milton Keynes, UK) confocal microscope with a Leica HCX PL APO CS 63x/1.4 NA oil immersion lens. FITC was excited with a 496 nm laser. Images were acquired and processed using Fiji ImageJ software (version 1.54f; National Institutes of Health, Bethesda, MD, USA)[40], as described in Athanasopoulos et al., 2015[18].

Time-course confocal laser microscopy (CLM) and hyphal growth rate measurements

The effect of each PEI-Cu compound on the hyphal growth rate was evaluated using confocal laser microcopy (CLM) images and subsequent image analysis. Conidia were inoculated into sterile ibidi 8-well coverslips. Each well contained 200 μL of MM and $\sim 5 \times 10^5$ *pabaA1* conidia mL^{-1}. The cells were incubated at 25 °C for 12–14 h. Following incubation, the cells in the ibidi chambers were transferred to the confocal microscope chamber, where 5 μg mL^{-1} of each of the test compounds was added separately, after which imaging started immediately thereafter. Time-course images were captured every 10 min over a 90-min period, with at least twenty individual cells measured per sample. Following image acquisition, hyphal growth rates were calculated using the MTrackJ plugin in Fiji ImageJ software (version 1.54f; National Institutes of Health, Bethesda, MD, USA) by measuring the elongation of individual cells in μm/min[41].

Epifluorescence and phase contrast microscopy

Coverslips containing the attached hyphal germlings of the *pabaA1* strain were imaged using an Axioplan 2 Observer Z1 fluorescence microscope (Carl Zeiss, Jena, Germany) equipped with a Plan-Apochromat 40× or 100×/1.40 NA oil immersion objective lens and appropriate fluorescent light filter sets. Images were captured with a digital camera (Retiga 2000R, QImaging, Surrey, BC, Canada) and Occular version 2.01 acquisition

software (Teledyne Photometrics, Inc., Tucson, AR, USA) and were processed with Fiji ImageJ software (version 1.54f; National Institutes of Health, Bethesda, MD, USA)[40].

Cytostatic effect of PEI-Cu complexes

To investigate the cytostatic effect of PEI-Cu complexes against *A. nidulans* quiescent conidia, ~10^6 *pabaA1* conidia mL^{-1} in 0.05% Tween-20 were cultured in 2 mL of MM supplemented with 5 mM urea, 1% (w/v) glucose and 5 μg mL^{-1} of each of the PEI-Cu complexes (PEI-Cu¼ or PEI–Cu$^1/_{16}$) tested. Cultures were grown on coverslips in 35 mm Petri dishes for 12–14 h at 25 °C. Cell images were captured using an Axioplan 2 fluorescence microscope, as previously described (see 2.10).

Mitochondrial morphology assay

To assess the impact of PEI-Cu complexes on the mitochondrial morphology of *A. nidulans* germlings, ~5×10^6 *pabaA1* conidia mL^{-1} in 0.05% (v/v) Tween-20 were cultured in 2 mL of MM supplemented with 5 mM urea and 1% (w/v) glucose as the sole nitrogen and carbon sources, respectively, in 35 mm Petri dishes containing a coverslip for 12–14 h at 25 °C. PEI, PEI-Cu¼ or PEI–Cu$^1/_{16}$ (5 μg mL^{-1}) was added, and the samples were incubated for an additional 5 and/or 15 min. For mitochondrial staining, 0.5 μM of the fluorescent probe MitoView™ 650 (Biotium) was added to each sample at least 15 min prior to imaging while protecting the samples from light exposure. Following staining, the coverslips with attached hyphal germlings were mounted onto microscope slides and visualized using an Axionplan 2 fluorescence microscope as previously described (see 2.10). The mitochondrial network of the cells was classified as tubular or nontubular (moderate or heavily fragmented), and the percentage of cells displaying a tubular mitochondrial network was measured for each sample. Approximately 200 cells were observed in each sample, and the experiment was repeated 3 times ($n = 600$).

Assessment of PEI-Cu complex stability

To assess the stability of PEI-Cu complexes and, consequently, the intracellular Cu^{2+} availability, a functional assay based on the pigmentation of *A. nidulans* conidia was used[42,43]. This approach is based on the requirement of copper for the activity of laccases, enzymes responsible for melanin synthesis in *A. nidulans* conidia (for more details, see results). In particular, *A. nidulans* ~ 10^6 *pabaA1* conidia mL^{-1} were inoculated into 96-well microplates containing 0.2 mL of copper-free liquid MM or each of the PEI-Cu complexes. The concentration of each polymer was adjusted to achieve a final copper concentration of 1.6 μM in each sample, equivalent to 0.8 μg mL^{-1} of PEI-Cu at a 1:4 ratio. Cultures were incubated at 37 °C for 90 min, plated on 35 mm Petri dishes containing copper-free MM and allowed to grow for 3–4 days at 37 °C. Subsequently, conidial pigmentation was observed.

Human cells, cell culture conditions and cell viability assay

Normal human skin fibroblasts (AG01523) used in this study were obtained from the Coriell Cell Repositories (Camden, NJ, USA). Cells were routinely cultured in DMEM supplemented with penicillin (100 U mL^{-1}), streptomycin (100 μg mL^{-1}) and 15% FBS and were regularly tested to ensure their mycoplasma-free status. Cultures were maintained in a humidified atmosphere at 37 °C and 5% CO_2, and cells were subcultured when necessary, using a trypsin/citrate (0.25%/0.30%, w/v) solution. The cell viability assay was performed as previously reported[44]. In brief, cells were cultured in 96-well plates until they became confluent. After the addition of PEI-Cu complexes at concentrations of 5–100 μg mL^{-1}, the cells were incubated for 4, 12 and 24 h. Putative cytotoxic effects of PEI and of $CuCl_2$ corresponding to the nominal copper ion concentration of the Cu: $N = 1{:}4$ derivative at the same concentrations were also assessed, while untreated cells served as the control samples. At the end of the incubation periods, the culture medium was aspirated and replaced with an MTT solution (1 mg mL^{-1} in phenol red-free DMEM), after which the cells were further incubated for 4 h. The resulting formazan crystals were dissolved in isopropanol, the optical density at 550 nm was measured using a Spark microplate analyzer (Tecan, Männedorf, Switzerland), and cell viability was estimated as the percentage of the untreated control. At least three independent experiments were performed in triplicate.

Statistical analysis

At least three independent repetitions were performed for each experiment, and the data are presented as the mean ± standard deviation. Student's t test was employed to assess statistical significance for all treatments (ns, * $p < 0.05$, ** $p < 0.01$, *** $p < 0.001$; ns not significant).

Results

Formation of PEI–Cu complexes

The coordination of $Cu^{2+}$with branched polyethyleneimine, which provides, to the best of our knowledge, the first polyamine-metal complex, was originally described in 1963[36] and has since been studied by many research groups[20,27–31,45–47]. Thus, it became evident that branched polyethyleneimines of different molecular weights and branched microstructures always form highly water soluble chelates with copper(II) ions; additionally, these materials have an intense blue color and exhibit a maximum in UV-Vis spectroscopy at 632–635 nm, with high stability constants[20,27–31,45–47]. However, PEI is a strong base, and at the concentrations employed throughout our experiments (up to 500 μg mL^{-1} in either minimal media or complete media for fungi or mammalian cells), the pH of the culture solutions was found to increase considerably. It was therefore necessary to employ phosphate buffer (PB, pH = 7.4, 100 mM) as well as to examine the conditions, specifically the molar ratio of Cu^{2+}:primary amino groups to PEI (Cu: N), that fully ensure complete binding of Cu^{2+} in this buffer to avoid any effects that could be due to the presence of free copper ions in our working solutions. To this end, we followed the formation

of the PEI-Cu complex using UV–Vis spectroscopy in PB, taking advantage of the strong absorbance of PEI-Cu solutions [both PEI solutions and free Cu^{2+} solutions at this wavelength and at the employed concentrations have negligible absorption]. The absorbance spectra follow the Beer–Lambert law and exhibit a maximum at 632 nm resulting from the $d_{xz/yz}$(Cu) -> $d_{x^2-y^2}$(Cu) charge transfer[48]. Consequently, complex formation in PB was followed by monitoring the absorbance of a PEI solution upon the addition of increasing quantities of Cu^{2+}. When PEI is present in excess, the absorbance is expected to be linear related to the Cu: N ratio, denoting the quantitative formation of the chelate, while when the absorbance deviates from the straight line, incomplete complex formation occurs, and uncompleted (free) Cu^{2+} are present[49,50]. As shown in Fig. S1A (Supporting Information), the absorbance maximum of all PEI- Cu^{2+} complexes was located at 632 nm, while by plotting the absorbance maximum vs. Cu: N molar ratio (see Supplementary Fig. S1B), the observed linearity indicated quantitative complex formation up to a 1:4 Cu: N molar ratio, which was, thereafter, the highest molar ratio employed in this study. Accordingly, PEI was not loaded with the maximum stoichiometric amount of Cu^{2+}, as usually employed in previous publications that study these complexes up to a ratio of Cu^{2+}:total number of PEI nitrogen groups equal to 4 or even to 5 (CuN4 and CuN5) due to the expected four-coordination or even five-coordination complexes[36,37,51–53]. Instead, we decided to work with solutions containing excess ligand to ensure complete binding of the Cu^{2+}. The registered absorbance maximum at 632 nm points to four atoms of N attached to each atom of $Cu^{2+}$and to a planar array of the four Cu^{2+}–N bonds (Fig. 1)[51,52,54,55]. PEI, due to its branched structure that contains primary, secondary, and tertiary nitrogen atoms, can be regarded not only as a homolog of linear ethylenediamine or triethylenetetramine[52] but also as a derivative of branched oligoamines, such as tris(2-aminoethyl)amine (tren)[51], all of which are known to form strong complexes with Cu^{2+} with planar geometry[29,30,49,50,56]. Therefore, it is reasonable to assume that Cu^{2+} is coordinated with the primary, secondary, and tertiary nitrogens of PEI, which can also explain the additional complex stability.

Dynamic light scattering experiments revealed a slight, however non-statistically significant increase in the polymer hydrodynamic size upon the addition of Cu^{2+} up to a Cu: N ratio of 1:16, which was also accompanied by a minor increase in zeta-potential (see Supplementary Fig. S2). Upon further increasing the Cu: N ratio, the zeta potential remains constant, while the size of the polymer is slightly reduced, although this size variation was again not statistically significant. The observed size and zeta potential increase is expected given that copper ion complexation within the hyperbranched scaffold would result in an increase in the overall positive charge and concomitant size increase of the polymeric nanoparticles due to electrostatic repulsion between the positively charged moieties. The slight decrease in size upon further addition of Cu^{2+} is most likely the result of the large number of Cu^{2+} complexes that formed, which caused the ethyleneimine branches to approach each other (Fig. 1), affording more compact nanoparticles.

Growth Inhibition of quiescent fungal cells by PEI–Cu complexes

The growth inhibitory effects of PEI-Cu¼ and PEI–Cu$^1/_{16}$ on quiescent conidiospores of the *A. nidulans* wild-type strain were investigated. Conidiospores in MM were treated with PEI-Cu¼ and PEI–Cu$^1/_{16}$ at near-MIC concentrations (Table 1) for 14 h at 25 °C, after which the ability to germinate and form mycelia was visually observed and was compared to that of untreated conidiospores. The results presented in Fig. 2 show that in the presence of the test PEI-Cu complexes, fungal conidiospores do not germinate to form hyphae, in accordance with our previously reported data obtained using PEI[13]. More specifically, compared with untreated conidiospores, treated conidiospores remain in the isotropic growth phase; this phase involves the establishment and maintenance of polarity and the eventual generation of the observed hyphae. These results suggest the growth-inhibitory effect of PEI-Cu¼ and PEI–Cu$^1/_{16}$. The MICs for the PEI-Cu complexes were estimated to be 6.5 ± 1 μg mL^{-1} for PEI–Cu$^1/_{16}$ and 5 ± 1 μg mL^{-1} for PEI-Cu¼, which are in the same range as that of PEI, as shown in Table 1.

Effect of PEI–Cu complexes on the viability of normal human skin fibroblasts

To exclude the possibility of undesirable cytotoxic effects of PEI-Cu complexes on normal human cells, we performed a cell viability assay in cells incubated with various concentrations of the complexes for 4, 12 and 24 h. Experiments were performed in a commercially available line of human skin fibroblasts, given the reported association of *A. nidulans* with cutaneous aspergillosis, especially in immunocompromised patients. As estimated by the MTT assay and shown in Fig. 3, a dose- and time-dependent cytotoxic effect induced by PEI-Cu complexes was observed. However, at concentrations up to 10 μg mL^{-1} of PEI-Cu¼ and PEI–Cu$^1/_{16}$ (which exceeds the MICs calculated for *A. nidulans*), human skin fibroblasts were shown to remain 100% viable and >90% viable after a 4- and a 12-h incubation, respectively. Even after a 24-h incubation, cells preserved approx. 90 and 80% viability at 5 and 10 μg mL^{-1}, respectively, of PEI-Cu¼ and PEI–Cu$^1/_{16}$. It should be noted that PEI was found to be slightly more cytotoxic than PEI-Cu complexes, whereas $CuCl_2$ was always non-cytotoxic to normal human skin fibroblasts. Similar results were obtained when the experiments were repeated using primary normal skin fibroblasts (data not shown).

Compound	MIC (μg mL^{-1})
PEI-Cu¼	5 ± 1
PEI–Cu$^1/_{16}$	6.5 ± 1
PEI	6.5 ± 1

Table 1. The minimum inhibitory concentrations (MICs) of the PEI-Cu¼ and PEI-Cu$^1/_{16}$ complexes.

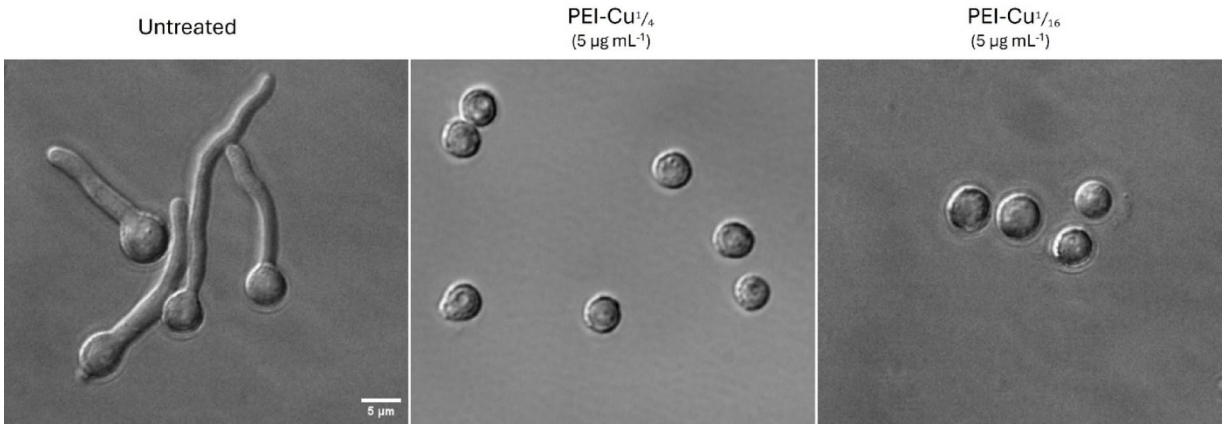

Fig. 2. Growth inhibitory effects of PEI-Cu¼ and PEI–Cu$^{1}/_{16}$ complexes against quiescent fungal cells of *A. nidulans*. Representative phase contrast microscopy images of *pabaA1* conidiospores grown for 14 h in the presence of 5 µg mL^{-1} PEI-Cu¼ or PEI–Cu$^{1}/_{16}$ at 25 °C.

Stability of PEI–Cu complexes

To assess the stability of the PEI-Cu complexes, conidial pigmentation was used as an indicator of intracellular copper abundance (see Materials and Methods). Briefly, in the absence of copper, defects in the dark green normal pigmentation of wild-type conidia most likely result from the absence of a functional copper-dependent laccase encoded by the *yA*$^{+}$ gene. This enzyme accumulates in the walls of conidia and converts a yellow precursor, an intermediate in the melanin biosynthesis pathway of *A. nidulans*, into melanin, resulting in dark green pigmentation[57]. During intracellular copper deficiency, laccase activity is impaired, as its polymerization is reduced, leading to the accumulation of a yellow intermediate[42]. Overall, conidial pigmentation serves as an indicator of intracellular copper availability, where dark green pigmentation indicates sufficient copper, while yellow pigmentation indicates copper limitation without affecting the growth rate of *A. nidulans* conidiospores.

When either PEI-Cu¼ or PEI–Cu$^{1}/_{16}$ was added to the copper-free growth MM, the natural green pigmentation was restored in *A. nidulans* conidia (Fig. 4). This result suggested that both PEI-Cu complexes dissociate (outside or/and inside the cell), releasing bioavailable copper ions that diffuse into the cytoplasm at concentrations sufficient to support copper-dependent laccase function, thus restoring normal dark green pigmentation. Despite the differences in copper content between PEI-Cu¼ and PEI–Cu$^{1}/_{16}$ complexes, a sub-MIC of 0.8 µg mL^{-1} was sufficient to initiate melanin production. This observation confirmed that copper is efficiently released from both complexes, rendering it accessible for cellular utilization, particularly under conditions of copper deficiency.

Effects of PEI–Cu complexes on the hyphal growth rate of *A. nidulans* germlings

Growth rate experiments of *A. nidulans* germlings were performed as described in Athanasopoulos et al., 2021[41]. Our results revealed that PEI, PEI-Cu¼, and PEI–Cu$^{1}/_{16}$ significantly inhibited the growth of germlings, as evidenced by the gradual decrease in the hyphal extension rate. Both PEI and PEI–Cu$^{1}/_{16}$ exhibited rapid cytostatic effects, stopping hyphal extension within 20–30 min of exposure. In contrast, PEI-Cu¼ had a delayed effect, requiring up to 90 min to completely stop hyphal extension, although a significant reduction in the overall growth rate, compared to that of untreated cells, was already observed from the first time point examined (10 min) (Fig. 5).

As further shown in Fig. 6, temporal differences in inhibition dynamics demonstrated the effect of copper on the antifungal activity of the test PEI polymers. Both PEI-Cu¼ and PEI–Cu$^{1}/_{16}$ showed a delayed cytostatic effect compared to that of PEI alone, suggesting that copper incorporation modulates the antifungal activity of PEI.

PEI–Cu complexes produce ROS in *A. nidulans* germinated conidia

To investigate the role of oxidative stress in the antifungal mechanism of PEI and PEI-Cu complexes, the accumulation of reactive oxygen species (ROS) in *A. nidulans* germinated conidia was evaluated. Using 2',7'-dichlorodihydrofluorescein diacetate (H_2DCFDA) in a fluorometric approach to detect ROS production, our results, shown in Fig. 7, revealed that PEI, PEI–Cu$^{1}/_{16}$, and PEI-Cu¼ significantly induced ROS production shortly after their addition, with significant DCF fluorescence detected within 5 min of incubation. The DCF fluorescence signal increased significantly 25 min after the cells were exposed to PEI and PEI-Cu complexes (Fig. 7). The rapid accumulation of ROS at 5 min preceded the cytostatic effects of the test compounds observed approximately 15–20 min after the cells were incubated at 25 °C (see Figs. 5 and 6), suggesting that oxidative stress could be one of the mechanisms underlying the antifungal activity of the compounds. However, ROS production is unlikely to be the primary mechanism, since the ROS scavenger *N*-acetyl cysteine NAC (10 mM) does not reverse or reduce the antifungal effects of PEI and PEI-Cu complexes (Fig. S4). Notably, at 25 min postexposure, PEI-Cu¼ showed a lower ROS signal than did PEI or PEI–Cu$^{1}/_{16}$, a result compatible with our data showing that in the presence of copper, the inhibitory effect of PEI on the fungal growth rate was significantly delayed (Figs. 5 and 6). In the presence of NAC, the DCF fluorescence was reduced under all the conditions

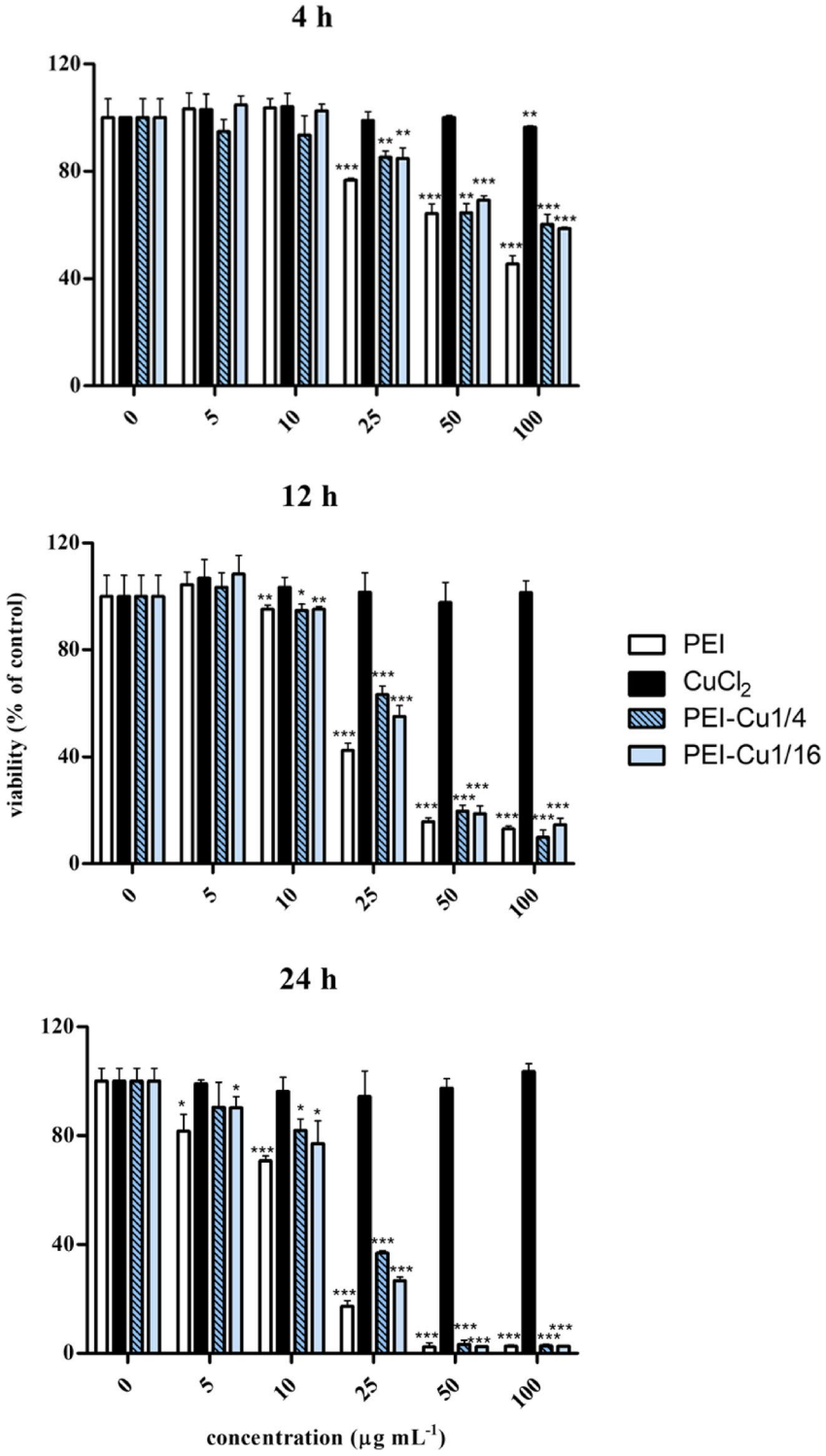

Fig. 3. Effect of PEI-Cu complexes on the viability of normal human skin fibroblasts, as estimated by the MTT assay. AG01523 cells were plated in 96-well plates until confluence, and PEI, PEI-Cu complexes and $CuCl_2$ corresponding to the nominal copper ion concentration of the Cu: N = 1:4 derivative were added at concentrations ranging from 0 (untreated control) to 100 µg mL^{-1} for 4, 12 and 24 h. At the end of the incubation periods, MTT was added at a concentration of 1 mg mL^{-1} for 4 h, and the optical density of the solubilized isopropanol formazan crystals was measured at 550 nm. Cell viability was calculated as a percentage of the untreated control samples. The data are presented as the mean values ± standard deviations. At least three independent experiments were conducted in triplicate with similar results. One representative experiment is shown here. Asterisks denote statistically significant differences in comparison to the respective control sample.

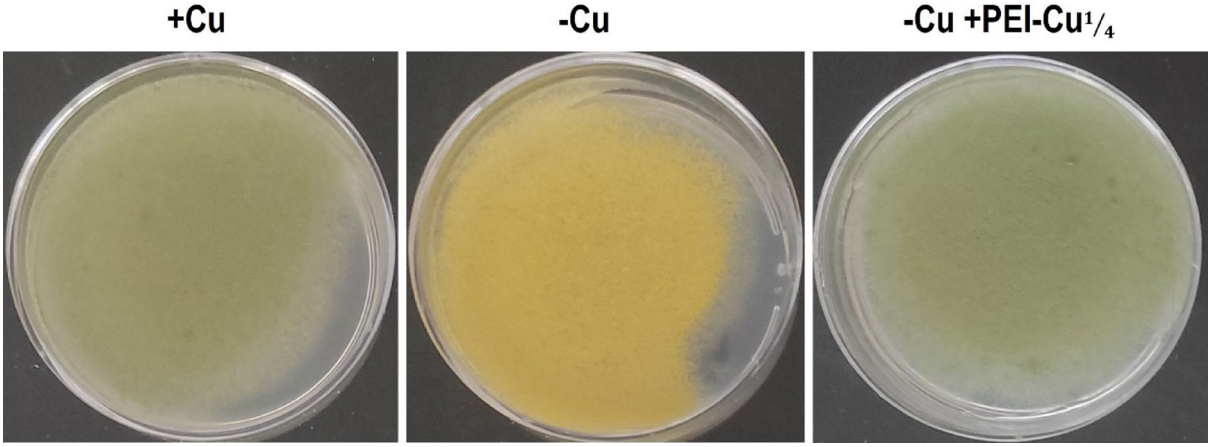

Fig. 4. Growth of *A. nidulans* conidiospores in copper-supplemented (+Cu) and copper-free (-Cu) minimal media. In the presence of copper, *A. nidulanspabaA1* conidia showed normal dark green pigmentation (left). In the absence of copper (-Cu), conidia exhibit yellow pigmentation due to reduced polymerization of copper-dependent laccases (middle). When 0.8 μg mL^{-1} of PEI–$Cu^{1}/_{16}$ was added to copper-free (-Cu) media, the conidia again showed normal dark green pigmentation (right). Similar results were observed with PEI–$Cu^{1}/_{16}$ (data not shown).

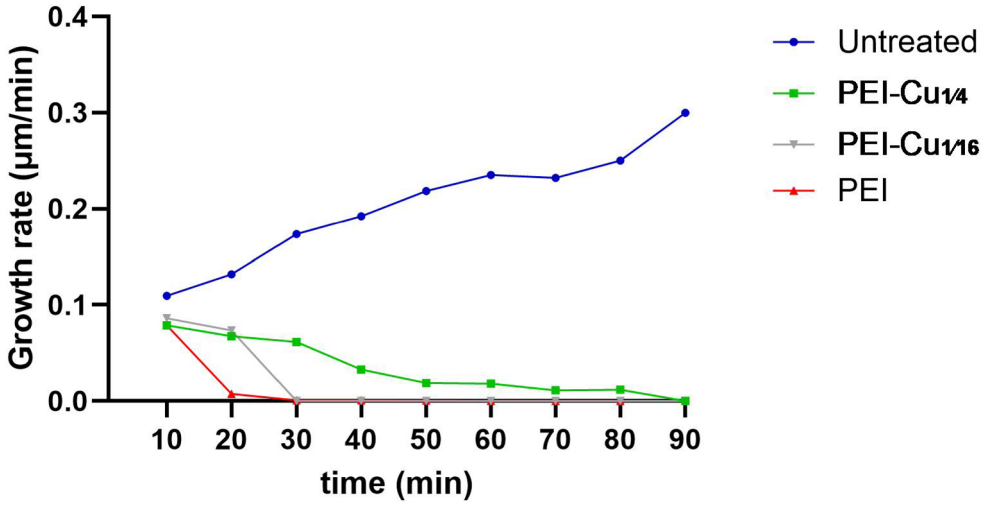

Fig. 5. Growth rate of *A. nidulans* 14 h germlings treated with 5 μg mL^{-1} PEI, PEI-Cu¼, or PEI–$Cu^{1}/_{16}$ at the indicated time points compared to untreated cells. Germlings were treated with PEI complexes for 90 min at 25 °C, and the hyphal growth rate (extension) was monitored using live microscopy and open-source software[41]. Dots represent the average hyphal extension velocity, calculated as the ratio of the distance the hyphal apical tip of the same germling moves between two consecutive microscopy frames (in μm) to the time interval between the frames (in min). All the polymers inhibited the hyphal growth rate, with PEI and PEI–$Cu^{1}/_{16}$ exhibiting cytostatic effects within 20–30 min and PEI-Cu¼ within 50–90 min. Data are expressed as a set of at least 30 independent hyphal extension velocity values (μm/min) obtained from at least 3 independent experiments.

tested. To further investigate whether ROS accumulation was associated with membrane damage, we performed propidium iodide (PI) staining to assess membrane permeability, as previously described[13]. PI staining revealed increased permeability in response to PEI-Cu complexes, supporting their involvement in membrane disruption (Fig. S3).

Effects of PEI–Cu complexes on mitochondrial morphology

To further investigate the involvement of oxidative stress in the mechanism underlying the antifungal activity of PEI and PEI-Cu complexes, we examined the morphology of the mitochondrial network, an indicator of the oxidative state of a cell, in *A. nidulans* germlings in the presence of each of the test compounds.

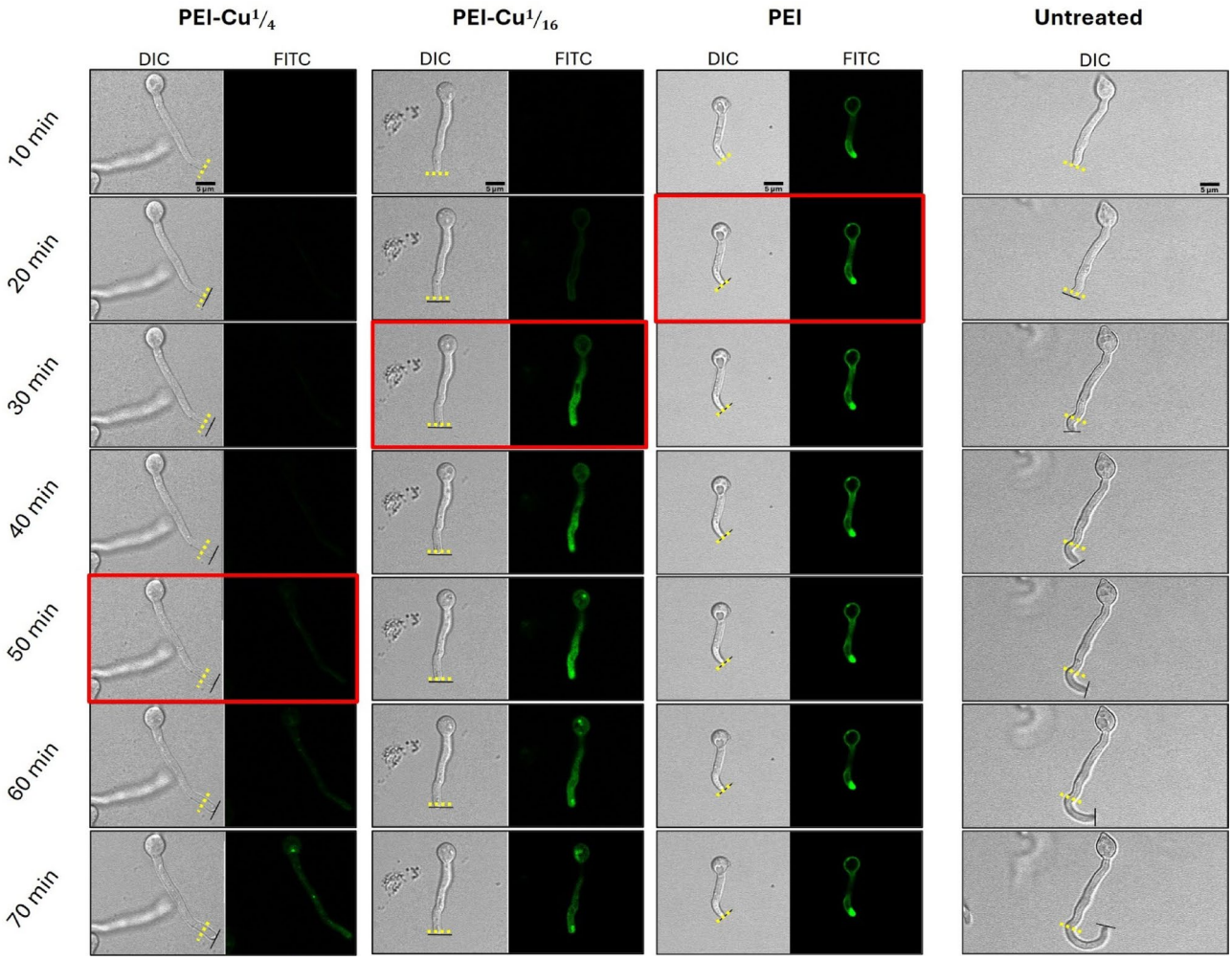

Fig. 6. Representative confocal microscopy images illustrating the time course of the hyphal growth rate in *A. nidulans* germlings treated with 5 µg mL^{-1} PEI-FITC, PEI-FITC-Cu¼ or PEI-FITC-Cu$^{1}/_{16}$ compared to that in untreated cells. Brightfield images (DIC) show hyphal extension over time, while the fluorescence channel (FITC) shows the localization of the fluorescein-labeled compounds. Yellow dotted lines indicate the initial position of the hyphal tip at the 10 min time point, while the black lines represent the current position of the hyphal tip at each subsequent time point. Frames outlined in red represent the time point at which the hyphal extension stopped, indicating growth inhibition. The hyphal extension of the depicted cells was stopped after 20 min of incubation with PEI-FITC, 30 min with PEI-FITC-Cu$^{1}/_{16}$ and 50 min with PEI-FITC-Cu¼, while growth continued in untreated cells. Accumulation of the test compounds, indicated by increased intracellular FITC-fluorescence, coincides with the onset of the inhibitory effect within a time window of approximately 10 min. The growth inhibition shown in the images reflects individual cell behavior; thus, these results may differ from the results for average extension velocity, as calculated from multiple hyphal measurements shown in Fig. 5. Scale bar: 5 µm.

To investigate this phenomenon, *pabaA1* germlings after 14 h of growth were exposed to 5 µg mL^{-1} PEI, PEI–Cu$^{1}/_{16}$ or PEI-Cu¼ for 5–15 min, subjected to MitoView labeling, and observed under a fluorescence microscope. A schematic representation and representative epifluorescence microscopy images of the distribution of the mitochondrial network in *A. nidulans* 14 h germlings visualized using Mitoview labeling are shown in Fig. 8a (for details, see the legend of Fig. 8). Analysis of epifluorescence microscopy images is presented as the percentage (%) of cells showing a tubular mitochondrial network (Fig. 8b) in comparison to cells with vesicular mitochondria. Furthermore, the results in Fig. 8b suggest a time-dependent increase in mitochondrial network fragmentation, indicative of increased oxidative stress. These early changes in mitochondrial network morphology, which precede the observed inhibitory effects of the test compounds on the apical growth rate (Figs. 5 and 6), suggest that mitochondrial function plays a role in the mechanism underlying the function of these compounds, possibly through the mediation of oxidative stress pathways.

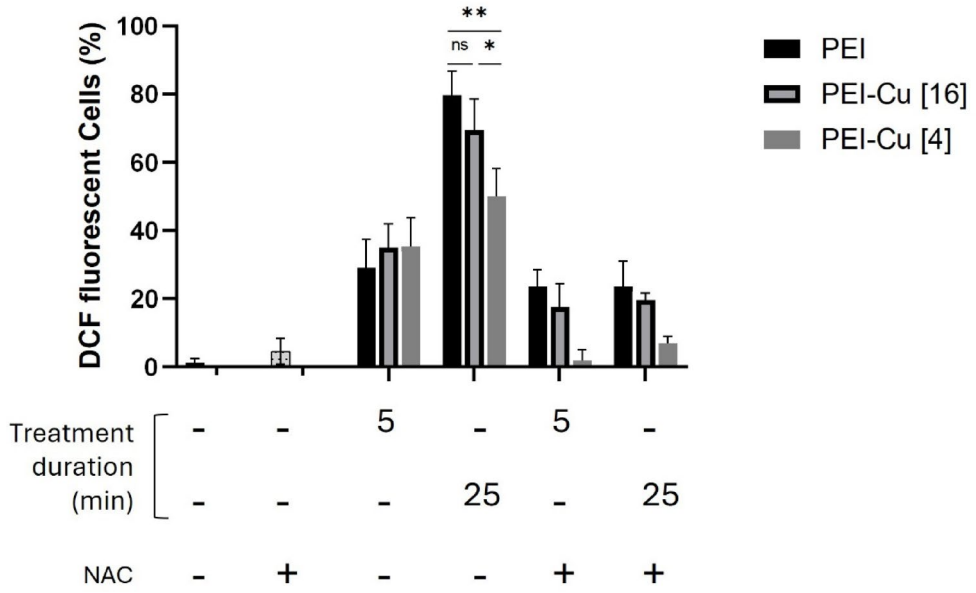

Fig. 7. Percentage of cells showing DCF fluorescence compared to the total number of cells observed under the indicated experimental conditions. *A. nidulans* germlings of 14 h growth at 25 °C were incubated for 5–25 min in the presence of 5 μg mL^{-1} PEI or PEI–Cu$^1/_{16}$ and PEI-Cu¼ complexes. The number of DCF-fluorescent cells was reduced in the presence of the ROS scavenger N-acetyl cysteine (NAC). Data are expressed as the mean ± SD of 3 independent values obtained from at least 3 independent experiments. A total of 450 cells were observed for each sample ($n = 450$). Asterisks denote statistically significant differences between the indicated data sets.

Cytotoxicity studies of PEI–Cu complexes against quiescent fungal cells

As quiescent fungal conidia are resistant to the currently available antifungals[26], the cytotoxicity of PEI-Cu complexes against *A. nidulans* quiescent conidia was evaluated. Based on our previously published data[17], a 2 h exposure period, starting immediately after conidia inoculation into the growth media, was chosen to target conidiospores in the quiescent state of their cell cycle[59]. A reduction in growth upon treatment with different PEI complexes was observed, calculated relative to the untreated conidia (control, defined as 100% growth). Conidial survival was significantly reduced to 27% of colony-forming units (CFUs) after treatment with PEI-Cu¼, compared to the 36% observed after treatment with PEI (Fig. 9). On the other hand, while PEI–Cu$^1/_{16}$ also significantly reduced quiescent conidia survival (34%), this reduction was not significantly different from that observed in PEI-treated conidia (Fig. 9).

A tenfold increase in the concentration of PEI–Cu$^1/_{16}$ or PEI-Cu¼ (50 μg mL^{-1}) further reduced conidial survival to approximately 12% and 13%, respectively, highlighting a dose-dependent effect. Moreover, extending the incubation time to 4 h and 6 h further enhanced the cytotoxic effects of all the test compounds at ~ MIC and ~ 10x MIC, emphasizing their time- and dose-dependent cytotoxic effects on quiescent fungal cells (Fig. 9).

Discussion

To guide research and development and increase public health awareness, in 2022, the WHO released the "WHO Focus priority Pathogens List"[5], which includes 19 different fungal pathogens divided into critical-, high-, and medium-priority groups. *Cryptococcus neoformans*, *Candida auris*, *Aspergillus fumigatus* and *C. albicans* are included in the so-called critical group of the WHO. This division is based mainly on the resistance of these pathogens to currently available antifungals. Although effective, existing antifungal drugs target mainly growing cells and operate via a narrow range of mechanisms, leading to rapid development of resistance. Based on the aforementioned knowledge, the development of novel antifungal agents with enhanced safety profiles is a priority for public health.

Our recent research showed that PEI has antifungal effects on *A. nidulans* quiescent conidia[13]. Furthermore, different cellular processes, such as stress responses, host invasion, commensalism, and antifungal sensitivity, were shown to be modulated by Cu^{2+} availability, as evidenced by the global gene expression dynamics under both copper depletion and excess copper, as determined via RNA-seq in the pathogenic fungus *C. albicans*[37]. Importantly, Cu^{2+} hypersensitivity has been reported for *C. albicans* mutants lacking the eisosome-resident protein Sur7, although the underlying molecular mechanism still remains elusive[60]. Given the antifungal properties of PEI and the relationship between metabolism and the antifungal sensitivity of the transition element copper, we chemically synthesized PEI copper chelates to examine their effect(s) on the antifungal properties of PEI.

Our results showed that both the PEI-Cu¼ and PEI–Cu$^1/_{16}$ complexes exhibited slightly greater fungicidal properties compared to PEI (Fig. 9). Importantly, no cytotoxic effects were observed on normal human skin

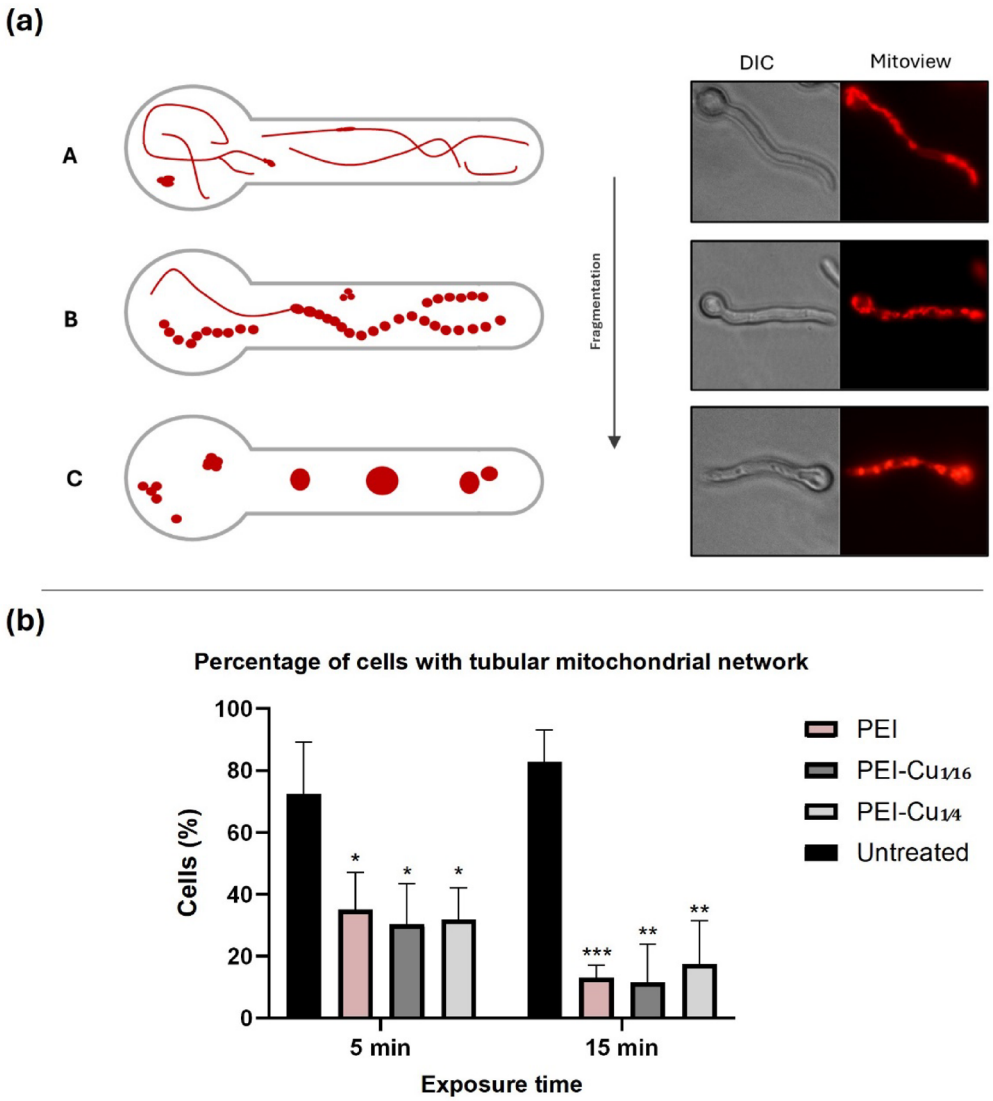

Fig. 8. Effects of PEI and PEI-Cu complexes on the mitochondrial morphology of *A. nidulans*. **a**) Schematic representation and representative epifluorescence microscopy images of the distribution of the mitochondrial network in *A. nidulans* 14 h-germlings, visualized using Mitoview labeling: (A) normal, filamentous/tubular mitochondrial network characterized by continuous, elongated mitochondrial structures forming interconnected tubules; (B) moderate fragmented network displaying a disrupted filamentous morphology with predominantly intermittent discontinuities (dotted lines); and (C) heavily fragmented network marked by large, distinct mitochondrial aggregates. These morphological variations reflect progressive changes in mitochondrial integrity. Tubular mitochondria indicate an intact mitochondrial network, indicative of low oxidative stress and normal cellular function[58]. **b**) Percentage of Mitoview-labeled cells displaying tubular mitochondria following 5- and 15-min exposures to 5 μg mL^{-1} PEI, PEI-Cu¼ or PEI–$Cu^{1}/_{16}$ at 25 °C. Data are expressed as the means ± SDs of 3 replicates obtained from at least 3 independent experiments. Asterisks denote statistically significant differences in comparison to the respective control sample.

fibroblasts at PEI or PEI-Cu complexes' concentrations up to 10 μg mL^{-1} or incubation times up to 12 h (Fig. 3), which were found to be entirely inhibitory for *A. nidulans*. It should be noted that normal human skin fibroblasts used in the present study represent an appropriate physiologically relevant in vitro cell model since *A. nidulans* has been implicated in cutaneous infections[15,16]. Lower survival rates of normal human skin fibroblasts were evident only by extending the range of PEI and PEI-Cu complexes' concentrations and/or incubation times, with concentrations ≥ 25 μg mL^{-1} (approx. 5-fold the MICs for *A. nidulans*) being considerably cytotoxic, especially over time (Fig. 3). A tendency of PEI-Cu¼ and PEI–$Cu^{1}/_{16}$ complexes to be less cytotoxic than the parent PEI though was shown here. As $CuCl_2$ was not cytotoxic even at the highest concentration or incubation time applied, the toxic effects on skin fibroblasts, when observed, may be attributed to PEI rather than copper, in accordance with the previously reported cytotoxic effect of PEI when used as a transfection agent in various

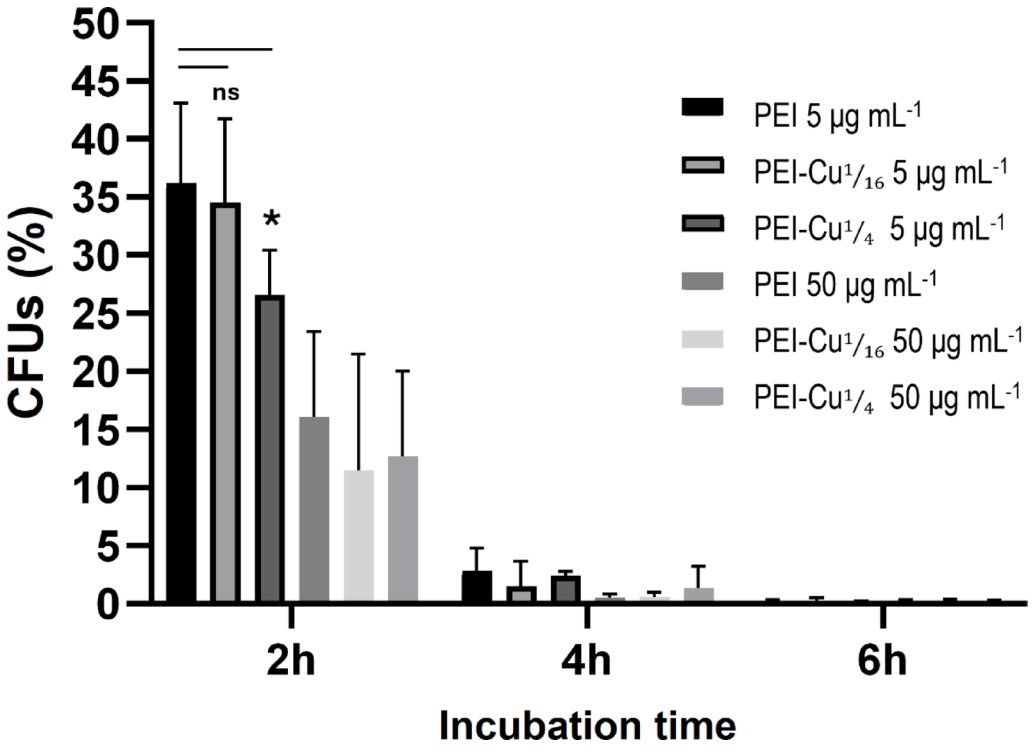

Fig. 9. Viability of *A. nidulanspabaA1* conidia, expressed as the percentage of colony-forming units (CFU), following treatment with 5–50 µg mL^{-1} (~ MIC and ~ 10x MIC) of PEI and PEI-Cu complexes at 2, 4, or 6 h. Colony counts were calculated for each case compared to those of untreated conidia (control), which was defined as 100% growth. Thus, relative viability was calculated as the percentage of survival of treated conidia compared to the untreated control. Data are expressed as the means ± SDs of 6 replicates obtained from at least 3 independent experiments. Asterisks denote statistically significant differences between the indicated data sets.

cell types[61]. In addition, copper has been reported to be beneficial for the skin, participating in the synthesis and stabilization of extracellular matrix proteins and angiogenesis[62].

Comparisons between PEI and its copper complexes showed that the higher the intracellular copper concentration was, the lower the sensitivity of germlings to antifungals was. Specifically, as demonstrated by the growth rate assay (Figs. 5 and 6), PEI-Cu¼ (a complex with a higher copper content) exhibited delayed antifungal activity compared to PEI–Cu$^{1}/_{16}$, suggesting that coordinated copper delays antifungal activity. The protective effect of copper on *A. nidulans* germlings is consistent with the corresponding reported data for *C. albicans*[37]. The delayed appearance of PEI-Cu¼ and PEI–Cu$^{1}/_{16}$ in fungal cells, as evidenced by their intracellular fluorescence compared to that of PEI (Fig. 6), suggested that copper modulates PEI internalization. However, once inside the cell, all the compounds caused inhibition within approximately 10 min (Figs. 5 and 6). This finding suggested that copper could affect cell membrane fluidity or permeability, internalization sites and/or the kinetics of the PEI uptake mechanism(s) rather than its intracellular function. The effect of PEI on the uptake mechanism could be associated with stress responses, as cells may actively alter their internalization pathways in response to metal exposure[63], or the bioactivity of PEI terminal groups could be reduced due to copper chelation, as reported for other functionalized derivatives[31]. Furthermore, our results showed that copper chelation enhances the fungicidal activity of PEI against quiescent conidia, as demonstrated by the conidial cytotoxicity assay (Fig. 9).

Regarding the mechanism of antifungal activity of PEI and PEI-Cu complexes, the differences in reactive oxygen species (ROS) production between *A. nidulans* germlings treated with PEI-Cu and those treated with the parent PEI (Fig. 7) suggest that an abundance of intracellular copper might protect fungal cells against oxidative stress. Despite the inherent ability of copper itself to induce ROS, intracellular ROS levels were significantly lower in hyphae treated with PEI-Cu¼ than in those treated with PEI[64,65]. Significant levels of ROS were detected shortly after exposure to PEI or PEI-Cu complexes, preceding the cytostatic effect, suggesting that oxidative stress is perhaps the cause of cellular death. ROS production within only 5 min is consistent with significant mitochondrial fragmentation, characterized by the transition from tubular to fragmented mitochondrial networks in *A. nidulans* germlings, further highlighting the importance of oxidative stress in the antifungal mechanisms of these compounds. Notably, both mitochondrial fragmentation and ROS accumulation are time dependent, indicating progressive and cumulative effects. Since oxidative stress pathways directly or indirectly affect mitochondrial function and vice versa[66–68], a link emerges between ROS production, mitochondrial dysfunction, and the antifungal activity of PEI and PEI-Cu complexes.

In conclusion, our findings suggest that the cytotoxic activity of PEI-Cu complexes against *A. nidulans* is mainly exerted by PEI, while Cu chelation seems to modulate PEI internalization. This could result in a delayed and controlled release of the fungicidal PEI in *Aspergillus* cells and explain the slightly lower toxicity of PEI-Cu complexes against mammalian cells, which is advantageous, especially in combination to the copper's reported property of being beneficial for the skin. In addition, PEI-Cu complexes could serve as metal-based probes providing higher specificity in their targets' recognition[69]. Finally, besides Cu-dependent delayed PEI internalization, we have shown that copper chelation slightly enhances the fungicidal activity of PEI against quiescent conidia. Further studies are needed to elucidate the molecular mechanisms underlying the antifungal activity of PEI and PEI-Cu complexes. In addition, a rational therapeutic scheme would be required in order to exploit PEI- and PEI-Cu complexes' antifungal activity on one hand and exclude putative undesirable side effects on infected human skin on the other, given that increasing concentrations and/or incubation times could result in cytotoxic effects also on normal human skin fibroblasts. Toward this direction, a periodical, short-term topical application on cutaneous surfaces could be suggested, e.g., by the incorporation of PEI and PEI-Cu complexes in appropriate cream formulations. Even more, advanced topical carriers could be employed to increase specificity and overcome existing challenges[70]. Furthermore, the study of new natural and/or synthetic putative antifungal metallopolymers could provide the basis for the development of additional antifungal agents that target both dormant and growing fungal cells via diverse mechanisms of action and are therefore more resilient to the development of fungal resistance.

Data availability

All data generated or analyzed during this study are included in this published article. All unique/stable reagents generated in this study are available.

Received: 24 January 2025; Accepted: 7 July 2025
Published online: 16 July 2025

References

1. Parums, D. V. & Editorial The world health organization (WHO) fungal priority pathogens list in response to emerging fungal pathogens during the COVID-19 pandemic. *Med Sci. Monit* **28**, e939088 (2022).
2. Fisher, M. C. & Denning, D. W. The WHO fungal priority pathogens list as a game-changer. *Nat. Rev. Microbiol.* **21**, 211–212 (2023).
3. Denning, D. W. Global incidence and mortality of severe fungal disease. *Lancet Infect. Dis.* **24**, e428–e438 (2024).
4. Zou, G. & Wei, Y. World health organization's first-ever release of a fungal priority pathogens list: A reply action proposal for the prevention and treatment of fungal pathogens. *Eco-Environ Health*. **2**, 43–44 (2023).
5. WHO data call for antifungal agents. doi: https://www.who.int/news-room/articles-detail/who-2024-data-call-is-now-open-for-antifungals-in-the-preclinical-development-pipeline (2024).
6. Berman, J. & Krysan, D. J. Drug resistance and tolerance in fungi. *Nat. Rev. Microbiol.* **18**, 319–331 (2020).
7. LaFleur, M. D., Qi, Q. & Lewis, K. Patients with Long-Term oral carriage harbor High-Persister mutants of *Candida albicans*. *Antimicrob. Agents Chemother.* **54**, 39–44 (2010).
8. Bojsen, R. et al. A common mechanism involving the Torc1 pathway can lead to amphotericin B-persistence in biofilm and planktonic *saccharomyces cerevisiae populations*. *Sci. Rep.* **6**, 21874 (2016).
9. Roemer, T. & Krysan, D. J. Antifungal drug development: challenges, unmet clinical needs, and new approaches. *Cold Spring Harb Perspect. Med.* **4**, a019703–a019703 (2014).
10. Ntow-Boahene, W. et al. Antifungal polymeric materials and nanocomposites. *Front. Bioeng. Biotechnol.* **9**, 780328 (2021).
11. Kumar, P. et al. Antimicrobial peptides: diversity, mechanism of action and strategies to improve the activity and biocompatibility in vivo. *Biomolecules* **8**, 4 (2018).
12. Velazco-Medel, M. A. et al. Antifungal polymers for medical applications. *Med. DEVICES Sens.* **4**, e10134 (2021).
13. Gerostathis, S. et al. Antifungal activity of functionalized hyperbranched polyethyleneimine derivatives against quiescent conidia and germlings of the opportunistic fungal pathogen *Aspergillus Nidulans*. *J Biol. Regul. Homeost. AGENTS* **38**, 2781–2794 (2024).
14. Henriet, S. S. V. et al. *Aspergillus Nidulans* and chronic granulomatous disease: A unique Host–Pathogen interaction. *J. Infect. Dis.* **206**, 1128–1137 (2012).
15. Van Burik, J. A. H. et al. Cutaneous aspergillosis. *J. Clin. Microbiol.* **36**, 3115–3121 (1998).
16. Lucas, G. M. et al. Primary cutaneous *Aspergillus Nidulans* infection associated with a Hickman catheter in a patient with neutropenia. *Clin. Infect. Dis.* **29**, 1594–1596 (1999).
17. Vangelatos, I. et al. Eisosome organization in the filamentous ascomycete *Aspergillus Nidulans*. *Eukaryot. Cell.* **9**, 1441–1454 (2010).
18. Athanasopoulos, A. et al. Characterization of AnNce102 and its role in eisosome stability and sphingolipid biosynthesis. *Sci. Rep.* **5**, 15200 (2015).
19. Athanasopoulos, A. et al. Fungal plasma membrane domains. *FEMS Microbiol. Rev.* **43**, 642–673 (2019).
20. Dzhardimalieva, G. I. & Uflyand, I. E. Synthetic methodologies and Spatial organization of metal chelate dendrimers and star and hyperbranched polymers. *Dalton Trans.* **46**, 10139–10176 (2017).
21. Festa, R. A., Thiele, D. J. & Copper An essential metal in biology. *Curr. Biol.* **21**, R877–R883 (2011).
22. Howlett, N. G. & Avery, S. V. Induction of lipid peroxidation during heavy metal stress in *Saccharomyces cerevisiae* and influence of plasma membrane fatty acid unsaturation. *Appl. Environ. Microbiol.* **63**, 2971–2976 (1997).
23. Salah, I. et al. Copper as an antimicrobial agent: recent advances. *RSC Adv.* **11**, 18179–18186 (2021).
24. Chatterjee, A. K. et al. Mechanism of antibacterial activity of copper nanoparticles. *Nanotechnology* **25**, 135101 (2014).
25. González, M. et al. Expression of copper-related genes in response to copper load. *Am. J. Clin. Nutr.* **88**, 830S–834S (2008).
26. Megarioti, A. H. et al. Ferroptosis-protective membrane domains in quiescence. *Cell. Rep.* **42**, 113561 (2023).
27. Paleos, C. et al. Multifunctional dendritic drug delivery systems: design, synthesis, controlled and triggered release. *Curr. Top. Med. Chem.* **8**, 1204–1224 (2008).
28. Gibney, K. A. et al. Poly(ethylene imine)s as antimicrobial agents with selective activity. *Macromol. Biosci.* **12**, 1279–1289 (2012).
29. Helander, I. M. et al. Polyethyleneimine is an effective permeabilizer of Gram-negative bacteria. *Microbiology* **143**, 3193–3199 (1997).
30. Azevedo, M. M. et al. Polyethyleneimine and polyethyleneimine-based nanoparticles: novel bacterial and yeast biofilm inhibitors. *J. Med. Microbiol.* **63**, 1167–1173 (2014).

31. Lykogianni, M. et al. Metabolomics reveals differential mechanisms of toxicity of hyperbranched poly(ethyleneimine)-derived nanoparticles to the soil-borne fungus *Verticillium dahliae* Kleb. *Pestic Biochem. Physiol.* **165**, 104535 (2020).
32. Mikula, P. et al. Branched Poly(ethylene imine)s as Anti-algal and Anti-cyanobacterial Agents with Selective Flocculation Behavior to Cyanobacteria over Algae. *Macromol. Biosci.* **18**, 1800187 (2018).
33. Fujimori, K. Complexation of poly(ethyleneimine) with copper(II) and nickel(II) ions in 0.5 M KNO_3 solution. *J. Polym. Sci. Polym. Chem. Ed.* **23**, 169–174 (1985).
34. Schlaepfer, C. W. & Zelewsky, A. V. Polymeric amines as ligands. Polyethyleneimines as ligands.in first and second coordination sphere. *Comments Inorg. Chem.* **9**, 181–199 (1990).
35. Treiber, C. et al. Cellular copper import by nanocarrier systems, intracellular availability, and effects on amyloid β peptide secretion. *Biochemistry* **48**, 4273–4284 (2009).
36. Grabchev, I. et al. Antimicrobial and anticancer activity of new poly(propyleneamine) metallodendrimers. *J. Polym. Res.* **24**, 210 (2017).
37. Khemiri, I. et al. Transcriptome analysis uncovers a link between copper metabolism, and both fungal fitness and antifungal sensitivity in the opportunistic yeast *Candida albicans*. *Front. Microbiol.* **11**, 935 (2020).
38. Heliopoulos, N. S. et al. Cytotoxicity effects of Water-Soluble Multi-Walled carbon nanotubes decorated with quaternized hyperbranched Poly(ethyleneimine) derivatives on autotrophic and heterotrophic Gram-Negative Bacteria. *Pharmaceuticals* **13**, 293 (2020).
39. Cao, X. et al. Core-shell type multiarm star poly(ε-caprolactone) with high molecular weight hyperbranched polyethylenimine as core: synthesis, characterization and encapsulation properties. *Eur. Polym. J.* **44**, 1060–1070 (2008).
40. Schindelin, J. et al. Fiji: an open-source platform for biological-image analysis. *Nat. Methods*. **9**, 676–682 (2012).
41. Athanasopoulos, A. et al. Quantitative analysis of *Aspergillus Nidulans* growth rate using live microscopy and Open-Source software. *J. Vis. Exp.* **62778** https://doi.org/10.3791/62778-v (2021).
42. Chang, P. K. et al. Biosynthesis of conidial and sclerotial pigments in Aspergillus species. *Appl. Microbiol. Biotechnol.* **104**, 2277–2286 (2020).
43. Scherer, M. & Fischer, R. Molecular characterization of a blue-copper laccase, TILA, of *Aspergillus Nidulans*. *FEMS Microbiol. Lett.* **199**, 207–213 (2001).
44. Konstantinou, D. et al. Bioprospecting Sponge-Associated marine Cyanobacteria to produce bioactive compounds. *Toxins* **12**, 73 (2020).
45. Dzhardimalieva, G. I. et al. Recent advances in metallopolymer-based drug delivery systems. *RSC Adv.* **9**, 37009–37051 (2019).
46. Zheng, Y. et al. Hyperbranched polymers: advances from synthesis to applications. *Chem. Soc. Rev.* **44**, 4091–4130 (2015).
47. Lederer, A., Burchard, W. H. & Polymers Macromolecules in between Deterministic Linear Chains and Dendrimer Structures. (*Royal Society of Chemistry, Cambridge*, https://doi.org/10.1039/9781782622468 (2015).
48. Wang, Z. & Urban, M. W. Facile UV-healable polyethylenimine–copper (C_2 H_5 N–Cu) supramolecular polymer networks. *Polym. Chem.* **4**, 4897–4901 (2013).
49. Perrine, T. D. & Landis, W. R. Analysis of polyethylenimine by spectrophotometry of its copper chelate. *J. Polym. Sci. [A1]* **5**, 1993–2003 (1967).
50. Papavasiliou, A. et al. Hyperbranched polyethyleneimine towards the development of homogeneous and highly porous CuO–CeO_2–SiO_2 catalytic materials. *Chem. Eng. J.* **300**, 343–357 (2016).
51. Stebani, U. et al. Metallomesogens with branched, dendrimeric amino ligands. *Angew Chem. Int. Ed. Engl.* **35**, 1858–1861 (1996).
52. Bew, M. J. et al. Electronic properties and stereochemistry of the copper(II) ion. Part VII. Mono(diethylenetriamine)copper(II) complexes. *J. Chem. Soc. Dalton Trans.* **1229** https://doi.org/10.1039/dt9720001229 (1972).
53. Tweedy, B. G. Plant extracts with metal ions as potential antimicrobial agents. *Phytopathology* **55**, 910–918 (1964).
54. Canonico, B. et al. Fine-Tuning the interaction and therapeutic effect of Cu(II) carbosilane metallodendrimers in Cancer cells: an *In vitro* Electron paramagnetic resonance study. *Mol. Pharm.* **17**, 2691–2702 (2020).
55. Sanz, D. et al. Insight into the antitumor activity of carbosilane Cu(ii)–metallodendrimers through their interaction with biological membrane models. *Nanoscale* **11**, 13330–13342 (2019).
56. Guerreiro, J. et al. Radiobiological characterization of $^{64}CuCl_2$ as a simple tool for prostate Cancer theranostics. *Molecules* **23**, 2944 (2018).
57. Aramayo, R. & Timberlake, W. E. The *Aspergillus Nidulans* yA gene is regulated by AbaA. *EMBO J.* **12**, 2039–2048 (1993).
58. Ruf, D., Brantl, V. & Wagener, J. Mitochondrial fragmentation in *Aspergillus fumigatus* as early marker of granulocyte killing activity. *Front. Cell. Infect. Microbiol.* **8**, 128 (2018).
59. Wang, F. et al. Transcription in fungal conidia before dormancy produces phenotypically variable conidia that maximize survival in different environments. *Nat. Microbiol.* **6**, 1066–1081 (2021).
60. Lanze, C. E. & Konopka, J. B. Sur7 mediates a novel pathway for $PI_{4,5}$ P_2 regulation in *C. albicans* that promotes stress resistance and cell wall morphogenesis. *Mol. Biol. Cell.* **35**, ar99 (2024).
61. Forcato, D. O. et al. Transfection of bovine fetal fibroblast with polyethylenimine (PEI) nanoparticles: effect of particle size and presence of fetal bovine serum on transgene delivery and cytotoxicity. *Cytotechnology* **69**, 655–665 (2017).
62. Borkow, G. Using copper to improve the Well-Being of the skin. *Curr. Chem. Biol.* **8**, 89–102 (2015).
63. Moraes, D. et al. Elsevier,. Molecular aspects of copper homeostasis in fungi. in *Advances in Applied Microbiology* **129** 189–229 (2024).
64. Weinstein, J. & Bielski, B. H. J. Kinetics of the interaction of perhydroxyl and superoxide radicals with hydrogen peroxide. The Haber-Weiss reaction. *J. Am. Chem. Soc.* **101**, 58–62 (1979).
65. Li, Y. et al. Iron and copper: critical executioners of ferroptosis, Cuproptosis and other forms of cell death. *Cell. Commun. Signal.* **21**, 327 (2023).
66. Bhat, A. H. et al. Oxidative stress, mitochondrial dysfunction and neurodegenerative diseases; a mechanistic insight. *Biomed. Pharmacother.* **74**, 101–110 (2015).
67. Shekhova, E. et al. Induction of mitochondrial reactive oxygen species production by itraconazole, terbinafine, and amphotericin B as a mode of action against *Aspergillus fumigatus*. *Antimicrob. Agents Chemother.* **61**, e00978–e00917 (2017).
68. Pan, Y. & Mitochondria Reactive oxygen species, and chronological aging: A message from yeast. *Exp. Gerontol.* **46**, 847–852 (2011).
69. Lakshmipraba, J. et al. Polyethyleneimine anchored copper(II) complexes: synthesis, characterization, in vitro DNA binding studies and cytotoxicity studies. *J. Photochem. Photobiol. B.* **142**, 59–67 (2015).
70. Garg, A. et al. Recent advances in topical carriers of anti-fungal agents. *Heliyon* **6**, e04663 (2020).

Acknowledgements

We thank Dr. A. Kolliopoulou for fruitful discussions and critical reading of the manuscript. We thank Prof. C. Scazzocchio for critical reading of the manuscript.This project is carried out within the framework of the National Recovery and Resilience Plan Greece 2.0, funded by the European Union - NextGenerationEU (Implementation body: HFRI, awarded to VS). Regarding infrastructure, it is supported by the project "An Open-Access Research Infrastructure of Chemical Biology and Target-Based Screening Technologies for Human and

Animal Health, Agriculture and the Environment (OPENSCREEN-GR)" (MIS 5002691) which is implemented under the Action "Reinforcement of the Research and Innovation Infrastructure", funded by the Operational Programme "Competitiveness, Entrepreneurship and Innovation" (NSRF 2014–2020) and co-financed by Greece and the European Union (European Regional Development Fund).

Author contributions

DT and ZS performed the synthesis and physicochemical characterization of the compounds. SG designed, performed and analyzed the experiments for the stabilization of the compounds and all other experiments in *A. nidulans* under the supervision of VS. EM and DK performed cell viability assays on normal human skin fibroblasts. SG, VS, EM, and DT prepared the manuscript. All authors contributed to manuscript editing and agreed on its content.

Declarations

Competing interests

VS is a member of the Editorial Board of the Scientific Report journal. I declare that VS has no access to any information regarding the peer review process of this manuscript. All other authors declare no conflict of interest.

Additional information

Supplementary Information The online version contains supplementary material available at https://doi.org/10.1038/s41598-025-11018-6.

Correspondence and requests for materials should be addressed to D.T. or V.S.